

Effect of spatial resolution of satellite images on estimating the greenness and evapotranspiration of urban green spaces

Hamideh Nouri¹  | Pamela Nagler² | Sattar Chavoshi Borujeni³ |
Armando Barreto Munoz⁴ | Sina Alaghmand⁵  | Behnaz Noori⁶ |
Alejandro Galindo⁷  | Kamel Didan⁴

¹Division of Agronomy, University of Göttingen, Göttingen, Germany

²U.S. Geological Survey, Southwest Biological Science Center, University of Arizona, Tucson, Arizona

³Soil Conservation and Watershed Management Research Department, Isfahan Agricultural and Natural Resources Research and Education Centre, AREEO, Isfahan, Iran

⁴Biosystems Engineering, The University of Arizona, Tucson, Arizona

⁵Department of Civil Engineering, Monash University, Clayton, Victoria, Australia

⁶College of Agriculture and Natural Resources, University of Tehran, Tehran, Iran

⁷Faculty of Engineering Technology, University of Twente, Enschede, the Netherlands

Correspondence

Hamideh Nouri, Division of Agronomy,
University of Göttingen, Von-Siebold-Strasse
8, 37075, Göttingen, Germany.
Email: hamideh.nouri@uni-goettingen.de

Abstract

Urban green spaces (UGS), like most managed land covers, are getting progressively affected by water scarcity and drought. Preserving, restoring and expanding UGS require sustainable management of green and blue water resources to fulfil evapotranspiration (ET) demand for green plant cover. The heterogeneity of UGS with high variation in their microclimates and irrigation practices builds up the complexity of ET estimation. In oversized UGS, areas too large to be measured with in situ ET methods, remote sensing (RS) approaches of ET measurement have the potential to estimate the actual ET. Often in situ approaches are not feasible or too expensive. We studied the effects of spatial resolution using different satellite images, with high-, medium- and coarse-spatial resolutions, on the greenness and ET of UGS using Vegetation Indices (VIs) and VI-based ET, over a 780-ha urban park in Adelaide, Australia. We validated ET with the ground-based ET method of Soil Water Balance. Three sets of imagery from WorldView2, Landsat and MODIS, and three VIs including the Normalized Difference Vegetation Index (NDVI), Enhanced Vegetation Index (EVI) and Enhanced Vegetation Index 2 (EVI2), were used to assess long-term changes of VIs and ET calculated from the different imagery acquired for this study (2011–2018). We found high correspondence between ET-MODIS and ET-Landsat ($R^2 > 0.99$ for all VIs). Landsat-VIs captured the seasonal changes of greenness better than MODIS-VIs. We used artificial neural network (ANN) to relate the RS-ET and ground data, and ET-MODIS (EVI2) showed the highest correlation ($R^2 = 0.95$)

This is an open access article under the terms of the Creative Commons Attribution License, which permits use, distribution and reproduction in any medium, provided the original work is properly cited.

© 2020 The Authors. *Hydrological Processes* published by John Wiley & Sons Ltd.

and $MSE = 0.01$ for validation). We found a strong relationship between RS-ET and in situ measurements, even though it was not explicable by simple regressions; black box models helped us to explore their correlation. The methodology used in this research makes a strong case for the value of remote sensing in estimating and managing ET of green spaces in water-limited cities.

KEY WORDS

evapotranspiration, EVI2, Landsat, MODIS, water consumption, WorldView

1 | INTRODUCTION

Newly emerged and still evolving concepts of “greening cities” and “moving towards carbon neutrality” are getting more attention in recent times. The benefits of urban green spaces (UGS) and their significance to public health and wellbeing are getting more recognized (Elgström, Erman, Klindworth, & Koenig, 2014; Li, Sutton, Anderson, & Nouri, 2017; Li, Sutton, & Nouri, 2018). The sustainable green city concept based on SDG-Goal 11 of “sustainable cities and communities” should not be limited to a narrow scope of only expanding UGS; sustainability scope must be expanded to the urban water system to avoid a possible conflict between “water-saving” and “greening cities” goals.

UGS are crucial elements in urban ecohydrology (linkage of water cycles and urban landscape) and their ecosystem services, which include their potential to mitigate climate change impacts and make cities more inhabitable and sustainable (Costanza & Liu, 2014; Wagner & Zalewski, 2009). Evaluation and enhancing their services require a better understanding of their metrics and indicators such as their extent and greenness, evapotranspiration (ET) and water use. These metrics help ecohydrological models to quantify the ecosystem services provided by UGS (Revelli & Porporato, 2018).

Water consumption, known as water lost to the atmosphere, or ET, takes a vital role in urban water management focused on UGS, particularly in dry regions where green plant covers are more affected by water scarcity and drought. In arid and semi-arid regions, UGS are mostly irrigated, thus making UGS a significant competitor for other water-demand sectors (Evans & Sadler, 2008; Nouri, Chavoshi Borujeni, & Hoekstra, 2019). Greenness, shading and ET play key roles in the cooling effect of the green spaces, and in mitigating the urban heat island (UHI) effects, and reduction of energy consumption. These roles mean that maintaining and expanding green plant covers of trees, shrubs and grasses require more water resources (Maheng, Ducton, Lauwaet, Zevenbergen, & Pathirana, 2019; Qiu et al., 2017; Skelhorn, Lindley, & Levermore, 2018). To balance urban greening and blue water saving, the water footprint of urban green cover – and in particular their ET, needs to be quantified.

There are numerous studies on the water use of UGS (Hilaire et al., 2008; Mini, Hogue, & Pincetl, 2014; Ouyang, Wentz, Ruddell, & Harlan, 2014). The majority of these studies refer to water withdrawal or water application/use of UGS rather than water consumption that is measured by ET. Total water consumption includes both blue water (irrigation water from surface and groundwater resources) and green

water (rainwater) (Nouri et al., 2019; Velpuri & Senay, 2017). The available literature on UGS ET estimation is mainly limited to small scales, for example, backyard gardens, due to the complication of making ET measurements in heterogeneous urban vegetation. For instance, an in situ method of soil water balance was established in an urban park in Adelaide – Adelaide Parklands – and was compared with three observational factor-based methods of Water Use Classifications of Landscape Species (WUCOLS), Irrigated Public Open Space program (IPOS), and Plant Factor (Nouri et al., 2016). Two factor-based approaches of Landscape Irrigation Management Program (LIMP) and WUCOLS were compared in two green spaces, a botanic garden and an urban forest in Isfahan, Iran (Shojaei, Gheysari, Nouri, Myers, & Esmaeili, 2018). Two methods of WUCOLS and portable chambers were used to measure ET from eight irrigated turfgrass regions in the Los Angeles Metropolitan area (Litvak, Bijoor, & Pataki, 2014; Litvak & Pataki, 2016). The outcomes of this later study were compared with an approach that calculates total ET by adding ET of both grasses and trees using empirical models and remote sensing maps of land covers (Litvak, Manago, Hogue, & Pataki, 2017). By this approach, a considerable portion of green shrubbery was not included in the total ET of these irrigated sites. This work did illustrate the necessity for proper spatial scale when assessing the ET of oversized UGS (i.e., UGS that are too large and complex to be studied by in situ approaches of ET estimation).

In the last two decades, remote sensing (RS) has introduced innovative approaches to measuring ET in large-scale regions, but it was primarily applied to agricultural systems, and to a lesser extent in riparian and lowland/upland forests, yet remote sensing-based ET has rarely been applied to UGS (Bastiaanssen, Menenti, Feddes, & Holtslag, 1998; Huete et al., 2002; Nagler et al., 2005; Nagler, Jarchow, & Glenn, 2018; Nouri, Beecham, Kazemi, & Hassanli, 2013; Su, 2002). Nouri, Beecham, Anderson, Hassanli, and Kazemi (2015) reviewed the potential of optical remote sensing to facilitate ET measurements in heterogeneous urban vegetation and later they employed remote sensing-based ET estimation methods in a small urban park (~10 ha) using high-resolution images of WorldView 2 & WorldView 3 (Nouri et al., 2017; Nouri, Beecham, Anderson, & Nagler, 2014).

Land cover mapping from free satellite imagery, such as MODIS, has been practised for decades (García et al., 2013; Yebra, Van Dijk, Leuning, Huete, & Guerschman, 2013). While free of charge, this class

of synoptic sensors is usually too coarse to accurately map UGS (Gómez, White, & Wulder, 2016; Grekousis, Mountakis, & Kavouras, 2015; Xian, Shi, Dewitz, & Wu, 2019). The high-frequency and high-quality MODIS data and VI time series (1–2 days) make it a promising tool to study vegetation change (greenness changes over time) in UGS, including their ET. Similarly, free images of Landsat with a higher spatial resolution (compared to MODIS) has the potential of supporting a more accurate estimation of green covers. Both of these advantages need to be tested in the context of an oversized urban landscape.

A new class of high-resolution, space-borne sensors, such as WorldView, IKONOS, Quickbird, and GeoEye with sub-meter resolution, can resolve biophysical parameters of the heterogeneous urban environment and bring a new dimension to the mapping of UGS. However, the cost of these images, their limited availability and footprint and associated processing make them not suitable for mapping of oversized UGS in cities.

In all remote sensing-based efforts, the Normalized Difference Vegetation Index (NDVI), the Enhanced Vegetation Index (EVI), and improved version of the Enhanced Vegetation Index 2 (EVI2), from high, medium and coarse resolution images, showed promising results in monitoring greenness and ET of large green covers in non-urban landscapes (Glenn, Neale, Hunsaker, & Nagler, 2011; Groeneveld, Baugh, Sanderson, & Cooper, 2007; Jarchow et al., 2020; Nagler et al., 2005). This research investigated the value of estimating greenness (VIs) and ET of oversized UGS using freely available remote sensing imagery. In this study, we evaluated the relationship between VIs from WorldView2, Landsat and MODIS and their VI-based ET for the oversized heterogeneous urban green space in order to understand the impact of spatial resolution. The aim was to: (a) compare different VIs from satellites with different spatial resolutions (WorldView2, Landsat and MODIS), (b) estimate the ET of large UGS using RS-ET methods and VIs, (c) assess the long-term intra- and inter-annual variations of VIs and ET, (d) compare RS-ET against the in situ ET method, (e) monitor changes in the greenness of the Adelaide Parklands, and (f) explore how local climate impacts of the VIs and ET on a seasonal scale.

This research study is timely as cities continue to explore carbon-neutral management strategies. Accurate estimation of the ET of large UGS is particularly important for Adelaide and other water-limited cities that have increasingly suffered from aridity and drought. These cities are rapidly expanding and are in pressing need for more proactive and sustainable water management strategies.

2 | STUDY AREA

The city of Adelaide is surrounded by green infrastructure known as the Adelaide Parklands (called “Parklands” in this study) consisting of 29 parks covering approximately 780 ha (Figure 1). The Adelaide Parklands is one of the largest urban parks in the world; it is almost three times larger than London's Hyde Park and is called “The heart and

lungs of Adelaide”. Over 510 plant taxa, about 40% native and 60% introduced species, are reported to exist in the Parklands. This diverse and distinctive landscape provides urban habitat for more than 150 species of birds, 33 species of mammal, 18 species of reptiles and six species of amphibian. This internationally unique green belt provides a precious social, environmental and recreational resource. Due to the expanse and heterogeneity of species, microclimate, plant density, and accessibility, we hypothesize that remote sensing data and tools would be a useful, practical for studying the water demand of this green belt.

3 | METHOD AND DATA

3.1 | Input data

3.1.1 | Satellite images

Three satellite sensors with different temporal and spatial resolutions of high-, medium- and coarse-pixel sizes were selected. These include WorldView2 (WV2), Landsat Operational Land Imager (OLI) and Thematic Mapper 5 and 7 (TM5 and ETM+), and Aqua MODIS; their relevant specifications are summarized in Table 1.

Worldview2 (8 bands, spatial resolution of 0.46 m panchromatic and 1.85 m multispectral); WorldView2 images were pre-processed (orthorectified and atmospherically corrected), NDVI from band 5 and 7 were calculated, and the Modifiable Areal Unit Problem (MAUP) effects on vegetation pixels in NDVI calculation were tested (Nouri et al., 2017). Bands 5 (red) and 7, near-infrared1 (NIR1), of WV2 were selected as the most accurate combination to calculate the ET of UGS (Nouri et al., 2014).

Landsat (ETM+ and OLI sensors with 11 bands, spatial resolution of 30 m); Landsat images were acquired for the period of 2011–2013 and 2013–2018, respectively. Landsat 8/OLI, data collection 1, Level-2 from Path 97 and Row 84 were obtained from the USGS Land Processes Distributed Active Archive Center (LP-DAAC) Earth Explorer (<https://earthexplorer.usgs.gov/>). Each scene consisted of individual GeoTIFF bands files (surfaces reflectance, VIs and pixel quality information). All scenes were then subset to a common geographic region of interest, and cloudy and poor quality pixels were removed based on the per-pixel QA information. Due to gaps in the data resulting from the Scan Line Corrector issue in Landsat 7 ETM+ (Storey, Scaramuzza, & Schmidt, 2005), we simply ignored the missing data and averaged whatever was present within the scene.

Aqua MODIS (with 36 bands, spatial resolution of 250 m for the red and NIR bands, 500 m for the remaining land bands, and 1 km for all other bands); MODIS Aqua data from tile h29v12 (collection 6) for the period 2011–2018 were downloaded from the LP DAAC (<https://lpdaac.usgs.gov/>) data pool.

All images were re-projected to a common geographic lat/lon grid using the WGS84 datum.

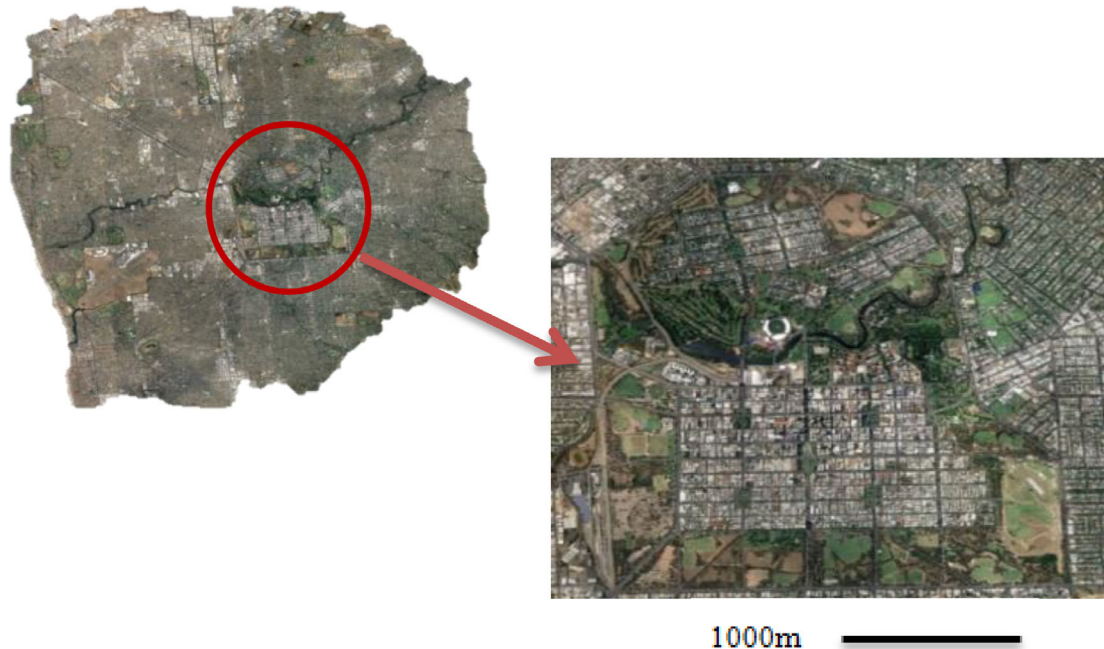


FIGURE 1 Adelaide Parklands in Adelaide, Australia (34.9403°S, 138.5930°E). The Park straddles the River Torrens and is centrally located serving the whole city. The park suffers continuous encroachment and land loss

3.1.2 | Meteorological data

Meteorological data for the Kent Town Station within the Adelaide Parklands (Station ID# 023090; Lat: -34.92, Lon: 138.62; Height: 48.0 m) were downloaded from the prerequisite dataset at the Bureau of Meteorology - BOM (www.bom.gov.au, last accessed date: 03.04.2019). The variables included precipitation, minimum temperature, maximum temperature, minimum relative humidity, maximum relative humidity, average wind speed and solar radiation.

3.2 | NDVI, EVI, and EVI2 vegetation indices

From a broad range of VIs (Barati, Rayegani, Saati, Sharifi, & Nasri, 2011; Glenn, Nagler, & Huete, 2010), NDVI, EVI, and EVI2 were selected to proxy the greenness of UGS in the Adelaide Parklands. NDVI, a normalized ratio of the NIR and red bands [Equation (1)], has been successfully used and established as a reliable monitoring and change detection tool of vegetation health and growth (Huete, Didan, van Leeuwen, Miura, & Glenn, 2011; Nagler et al., 2016; Nguyen, Glenn, Nagler, & Scott, 2015).

$$\text{NDVI} = \frac{\text{NIR} - \text{Red}}{\text{NIR} + \text{Red}}. \quad (1)$$

The EVI was designed to complement NDVI over denser canopies with more sensitivity as a result of the de-coupling of the canopy background signal and a reduction in atmosphere influences (Huete

et al., 2002; Glenn et al., 2015). Similar to NDVI, EVI uses a ratio of NIR, red, and blue bands [Equation (2)].

$$\text{EVI} = G \times \frac{\text{NIR} - \text{Red}}{\text{NIR} + C1(\text{Red}) - C2(\text{Blue}) + L}. \quad (2)$$

The coefficients adopted in the MODIS-EVI algorithm are $L = 1$, $C1 = 6$, $C2 = 7.5$ and G (gain factor) = 2.5.

EVI2, a two-band EVI version (Jiang, Huete, Didan, & Miura, 2008; Kim, Huete, Miura, & Jiang, 2010) removes the blue band from the formulation to address the lack of blue band and/or blue bandpass variation across sensors. EVI2 is functionally the same as EVI (Jiang et al., 2008) is expressed as [Equation (3)].

$$\text{EVI2} = 2.5 \times \frac{\text{NIR} - \text{Red}}{\text{NIR} + 2.4(\text{Red}) + 1}. \quad (3)$$

A binary geographic mask, containing only the boundary of the Parklands, was created for WorldView2 (1.85 m), Landsat (30 m) and MODIS (250 m), respectively, using a majority intersection method, where if a pixel spills outside the area only those pixels with more than 50% overlap are retained. This mask was then used to indicate which pixels within the overlapping area from each MODIS and Landsat scene are to be used in further analysis. A data filtering mask based on the per-pixel QA was applied to all scenes, and only clear and low-aerosol-load observations were retained. To limit hypersensitivity to data noise, especially in ETM and OLI data, we implemented a statistical filtering strategy that removes all outliers, which are

TABLE 1 Specifications of three types of satellite imagery from MODIS, Landsat and WorldView2

Specifications	Landsat			WorldView2	
	MODIS	OLI	ETM+		
Number of bands	36 (7 bands of land/cloud/aerosols)	11	8		8
Spectral resolution (m)	250 bands 1 and 2,500 bands 3–7	15 m panchromatic, 30 m multispectral cirrus, 100 m thermal	15 m panchromatic, 30 m multispectral, 60 m thermal	46 cm panchromatic, and 1.84 m multispectral	
Band ranges (μm)					
Band 1	0.62–0.67	Band 1 - coastal aerosol	0.43–0.45	1. 0.45–0.515	30
Band 2	0.841–0.876	Band 2 - Blue	0.45–0.51	2. 0.525–0.605	30
Band 3	0.459–0.479	Band 3 - Green	0.53–0.59	3. 0.63–0.69	30
Band 4	0.545–0.565	Band 4 - Red	0.64–0.67	4. 0.775–0.90	30
Band 5	1.230–1.250	Band 5 - NIR	0.85–0.88	5. 1.55–1.75	30
Band 6	1.628–1.652	Band 6 - SWIR 1	1.57–1.65	6. 104–12.5	60
Band 7	2.105–2.155	Band 7 - SWIR 2	2.11–2.29	7. 2.08–2.35	30
		Band 8 - panchromatic	0.50–0.68	8. 0.52–0.9	15
		Band 9 - Cirrus	1.36–1.38		NIR2
		Band 10 - TIRS 1	10.6–11.19		Panchromatic
		Band 11 - TIRS 2	11.50–12.51		0.45–0.77

observations that stray far away from the normal trends in the data using an envelope of $\pm 1.5 \sigma$ (standard deviation). And while this data filtering strategy tends to be too conservative, we hypothesised that sacrificing good observations is more prudent than ingesting poor quality data. A long-term (2011–2018) average profile for each pixel in the Parkland was generated using the simpler QA filtering approach described above. Any observation that falls outside the $+/-1.5\sigma$ envelope is then removed unless the deviation persists in subsequent images, which indicates disturbance and not noise.

Furthermore, Landsat 8 (OLI) and Landsat 7 (ETM+) have slightly different NDVI dynamic ranges, and scales, which creates bias. To address this bias and correct the range and scale issues, we removed discontinuity across sensors by applying a seasonal-based, per-pixel, across-sensors continuity-transfer equation modelled using 4 years of overlap between OLI and ETM+ (2013–2016). These continuity functions were simple linear regression models that relate the two sensors and were applied to all ETM+ datasets to create an OLI like data record for years 2011 and 2012, effectively creating a sensor independent, seamless, OLI like time series. Any resulting temporal gaps were interpolated from adjacent observations.

3.2.1 | Vegetation index scaling

To address scene-to-scene variability resulting from atmosphere correction and/or sun and viewing geometry, we removed NDVI outliers at the high and low ends, by calculating the max/min NDVI values for each scene using barren soil or verdant (green vegetation) pixels, typically from agricultural fields (Groeneveld et al., 2007). We identified the barren soil area within the scene and averaged all NDVI pixels to generate the NDVI_{\min} . Similarly, using verdant agricultural fields in the scene, we determined the absolute highest NDVI value; we then averaged all pixels within 95% of that absolute value to generate NDVI_{\max} . This process was only applied to NDVI following Jarchow, Didan, Barreto-Muñoz, Nagler, and Glenn (2018). A scaled Landsat NDVI* was then computed using Equation(4).

$$\text{NDVI}^* = \frac{(\text{NDVI} - \text{NDVI}_{\min})}{(\text{NDVI}_{\max} - \text{NDVI}_{\min})}. \quad (4)$$

Equation (4) is the fractional vegetation cover (Gutman & Ignatov, 1998; Jiapaer, Chen, & Bao, 2011; Montandon & Small, 2008; Zeng et al., 2000; Zhang, Liao, Li, & Sun, 2013); however, in this work, it is used to scale the NDVI value in order to remove the scene-to-scene variation related to variable atmosphere and observation conditions.

3.3 | ET computation

We estimated the greenness using NDVI, EVI, and EVI2 and then calculated ET by Equations (5) and (6) (Nagler, Glenn, Nguyen, Scott, & Doody, 2013).

$$ET = ET_0 * 1.65 \left(1 - e^{-2.25 * EVI \text{ (or } EVI2)}\right) - 0.169. \quad (5)$$

The ET_0 refers to the reference ET defined as “the rate of evapotranspiration from a hypothetical reference crop with an assumed crop height of 0.12 m, a fixed surface resistance of 70 sec m⁻¹ and an albedo of 0.23, closely resembling the ET from an extensive surface of green grass of uniform height, actively growing, well-watered, and completely shading the ground” (Irmak & Haman, 2003). Daily ET₀ data were acquired from the Kent-Town weather station in Adelaide. EVI and EVI2 were calculated from Equations (2) and (3).

Landsat NDVI based ET was calculated using Equation (6) (Nagler, Nguyen, et al., 2018; Nagler, Jarchow, & Glenn, 2018) as a function of reference ET (ET₀) and scaled NDVI from Equation (4).

$$ET = ET_0 * NDVI^*. \quad (6)$$

The long-term trend and correlation between RS-ET including ET-MODIS (EVI), ET-MODIS (EVI2), ET-Landsat (NDVI), ET-Landsat (EVI) and ET-Landsat (EVI2) during 2011–2018 within the study area were investigated.

3.4 | Ground data

The ground data were collected using the soil water balance (SWB) method to quantify the main components of the water budget equation (Glenn et al., 2013). ET was calculated from the mass balance of water inflows and outflows over the study period using in situ measurements from the experimental site; a full description of the methodology and data are available from Nouri et al. (2016).

Water balance in the root zone, for a given time period, is calculated by Equation (7).

$$P + IR - ET - DR - RO + CR = \Delta S, \quad (7)$$

where P is precipitation, ET is evapotranspiration, IR is irrigation, DR is drainage, RO is runoff and ΔS is the change in soil moisture status.

To capture the heterogeneity of landscape plant species, density and microclimate within the Parklands, two layers of data for soil salinity – using proximal sensing by electromagnetic – EM38 – and landscape cover – using airborne images to differentiate turfgrasses from trees and shrubs – were overlapped and four sampling zones were defined. These four zones included 1 – low salinity (<1.2 dS/m) – primarily covered with turf grasses with few trees and shrubs, 2 – high salinity (>1.2 dS/m) – primarily covered with turf grasses with few trees and shrubs, 3 – low salinity (<1.2 dS/m) – mostly trees and shrubs with intermittent turf grasses, and 4 – high salinity (> 1.2 dS/m) – mostly trees and shrubs with intermittent turf grasses. Samples for drainage and soil moisture status were collected from these four zones, and the average was assumed a representative for the full site.

Meteorological data were acquired from two stations, an in situ wireless weather station in the Parkland and the closest station of the

Australian Bureau of Meteorology (BOM, 34.92°S, 138.62°E; Elevation 48 m) which is located 2.9 km from the Parklands. Precipitation data (P) were recorded by these weather stations. Four zero-tension pan lysimeters were installed in the Parkland to monitor drainage quality and quantity (DR). Details of design, structure, installation, data collection and maintenance of these lysimeters were fully described by Nouri, Beecham, Hassanli, and Ingleton (2013). The capillary rise (CR) was monitored every 3 months through monitoring wells. Soil moisture status (δS) was regularly measured by the in situ method of neutron moisture meter (NMM) in different soil depths, down to 4-m, at 12 points in the study site. Irrigation data (IR) were obtained from the local authority, Adelaide City Council. Monthly ET was estimated as the residual in the SWB equation by monitoring the inflows, precipitation, irrigation and capillary rise, and outflows – runoff, drainage, and soil moisture.

3.5 | Comparison of RS-ET and ground data

To relate RS-ET dataset to in situ measurement, both, linear and non-linear, approaches of modelling were studied and compared. In modeling domains, linear regression technique has well-known optimization strategies that tend to the significant outcome, when the underlying relationship between input/output variables is linear. While neural networks usually outperform linear regression where the linear approximation is not valid, that is, the nature of data is unknown, complex and non-linear. Neural networks are versatile, more flexible and resistant to outliers and use nonlinear activation functions to handle multidimensional dependencies of data. They can be employed as an efficient alternative to the linear regression when the model performance is evaluated only based on “goodness of fit” criteria without the need to interpret the model. Regression models were not well-suited for these relationships; hence a black box approach was employed to develop a prediction model. A feedforward multi-layer perceptron (MLP), with backpropagation learning algorithm, was used to model the relationship between SWB and ET from Landsat and MODIS. Several inputs including different combination of ET-Landsat (NDVI), ET-Landsat (EVI), ET-Landsat (EVI2), ET-MODIS (EVI) and ET-MODIS (EVI2), in addition to varying numbers of hidden layers (1–5), different number of neurons per hidden layer (1 to 10), and several activation functions (Sigmoid or Logistic, Linear, Tanh or hyperbolic tangent), as well as numerous scenarios (architectures) were defined and tested, and their performances were compared. To ensure successful modelling with MLPs, an important generalization step was considered. The Levenberg–Marquardt algorithm, the modification of the classic Newton algorithm for finding the optimum solution, was employed as the most common method for adjusting the weights in the MLP and training the network. The dataset, including input and output, were initially normalized over the range of [0,1] and divided into two random subsets of calibration (80% of data), and validation (20% of data). The calibration set was used to find the parameters of the optimum MLPs and the validation set was employed to check the generalization potential of the selected MLPs.

The performances of scenarios were evaluated by conventional statistical criteria of goodness of fit, including mean squared error (MSE), and the coefficient of determination (R^2) using Equations (8) and (9).

$$MSE = \frac{E_i - \hat{E}_i}{n} \quad (8)$$

$$R^2 = \left[\frac{\sum_{i=1}^n (E_i - \bar{E}_i) \cdot (\hat{E}_i - \tilde{E}_i)}{\sqrt{\sum_{i=1}^n (E_i - \bar{E}_i)^2 \cdot \sum_{i=1}^n (\hat{E}_i - \tilde{E}_i)^2}} \right]^2, \quad (9)$$

where E_i , \hat{E}_i , \bar{E}_i and \tilde{E}_i are the observed, simulated, mean of observed and mean of simulated values, respectively, and n denotes the number of data.

The training phase stops when the mean square error (MSE) reaches zero, or a predefined maximum number of epochs is reached. A MATLAB code was developed to run these models. The optimum MLP topology was determined by trial and error, including an input layer (SWB), one hidden layer (with varying number of neurons in different optimum scenarios), one output layer (an individual satellite index in each individual scenario), tangent hyperbolic transfer function, and Levenberg–Marquardt learning algorithm.

4 | RESULTS

4.1 | Vegetation indices from WV2, Landsat and MODIS

4.1.1 | Time series of VIs from Landsat and MODIS (2011–2018)

Long-term trends of NDVI, EVI, and EVI2 from Landsat and MODIS (2011–2018) were investigated. Time series of VIs helped to explain the variation of greenness throughout the year and observe seasonal changes of UGS. All VIs, those from Landsat (NDVI), Landsat (EVI), Landsat (EVI2), MODIS (NDVI), MODIS (EVI), and MODIS (EVI2), showed inter- and intra-annual variations (Figures 2 and 3). Seasonal variations were better captured by the finer Landsat-VIs time series compared to MODIS. Intra-annual graphs of NDVI, EVI and EVI2 from Landsat revealed that from January all VIs monotonically increased over summer and autumn to peak in winter (July–August) and slowly dipped to their lowest values in December, corresponding to the beginning of summer time in Adelaide. Medians of NDVI, EVI and EVI2 from Landsat varied from 0.55 to 0.36 to 0.34, respectively. For Landsat, NDVI presented the largest range in amplitude and reached 0.70 towards late June. Year-to-year variations of VIs in Landsat were relatively similar except during the following times: EVI2 in November 2011, both NDVI and EVI in May 2016, and all three VIs, NDVI, EVI and EVI2, in January 2017.

The seasonal profiles and changes derived from MODIS were not as strong or well-defined, likely due to pixel mixing resulting from the larger pixel sizes. Inter-annual variations from year-to-year were relatively similar. Medians of NDVI, EVI and EVI2 varied from 0.49 to 0.32 to 0.29, respectively; NDVI showed the largest range that reached to 0.68 towards mid-July (Figure 3).

4.1.2 | Comparison of NDVI from WorldView2, Landsat, and MODIS

A set of five cloud-free WorldView2 (WV) images (March 18, 2012, June 29, 2012, August 17, 2012, November 9, 2012, and January 16, 2013) over the Parklands were pre-processed and compared with Landsat and MODIS imagery. The WV2 images covered only the southern half of the Parklands; additional images were not acquired due to the prohibitively high cost. To compare NDVI from WV with Landsat and MODIS, we clipped Landsat and MODIS images to match the coverage of WV2 scenes (Figure 4). NDVs from these three sources of imagery were compared; the closest values were seen in March, where WV2-NDVI was slightly higher than Landsat-NDVI and marginally lower than MODIS-NDVI. For the rest of the year, Landsat had the highest NDVI, and WV the lowest, but closer to MODIS.

4.2 | Comparison of RS-ET

The trends of ET from time-series data produced using EVI, EVI2 and NDVI from Landsat (ETM+ and OLI) and MODIS for the period 2011–2018 were observed, and their correlations were tested. The correlation between ET-MODIS (EVI) and ET-MODIS (EVI2) was very high ($R^2 = 0.99$; $p < .05$). ET-MODIS (EVI) ranged from 0.44 to 7.57 with a mean of 2.9, and mean SD of 0.72 compared to ET-MODIS (EVI2) that ranged from 0.41 to 7.16 with a mean of 2.72, and mean SD of 0.67. ET-MODIS (EVI) was consistently higher than ET-MODIS (EVI2). Both ET estimates were lowest in June and July (wintertime in Adelaide) and largest in December and January (summertime in Adelaide).

The correlation between ET-Landsat (NDVI), ET-Landsat (EVI) and ET-Landsat (EVI2) was very high ($R^2 = 0.99$; $p < .05$) with a range of 0.91–9.57 (mean 4.00 and mean SD 0.85) for ET-Landsat (NDVI) compared to a range of 0.64–7.54 (mean 3.03, and mean SD 0.92) for ET-Landsat (EVI), and a range of 0.61–7.26 (mean 2.89, and mean SD 0.91) for ET-Landsat (EVI2). ET-MODIS (EVI) was consistently higher than ET-MODIS (EVI2).

ET from Landsat and MODIS were lowest in June, July, and August, the winter in Adelaide, and highest in late November, December, January, and sometimes early February, the summer in Adelaide (Figures 5 and 6). Comparing ET from Landsat, ET-Landsat (NDVI) was consistently highest, and ET-Landsat (EVI2) was lowest. These trends had substantial agreements with observational methods of ET estimation in the Parklands (Nouri, Beecham, Hassanli, & Kazemi, 2013) and our ground data. Irrigation of the Parklands usually stops in winter; water resource for the Parklands in winter is limited to green water.

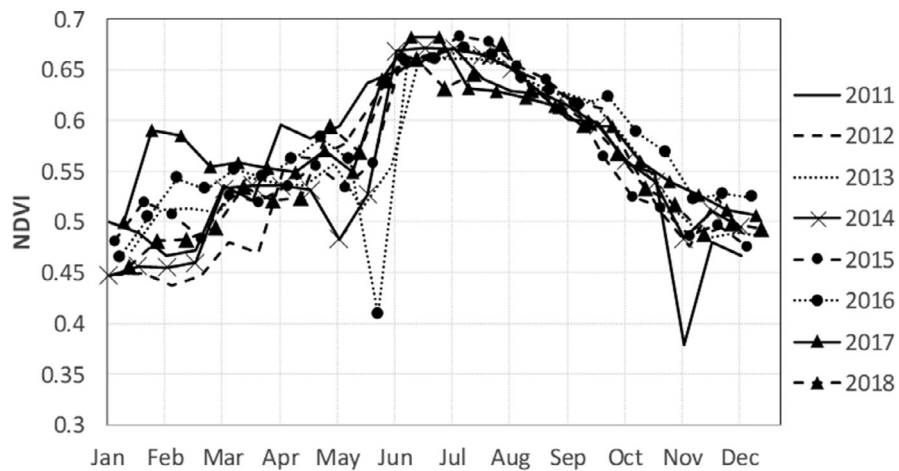
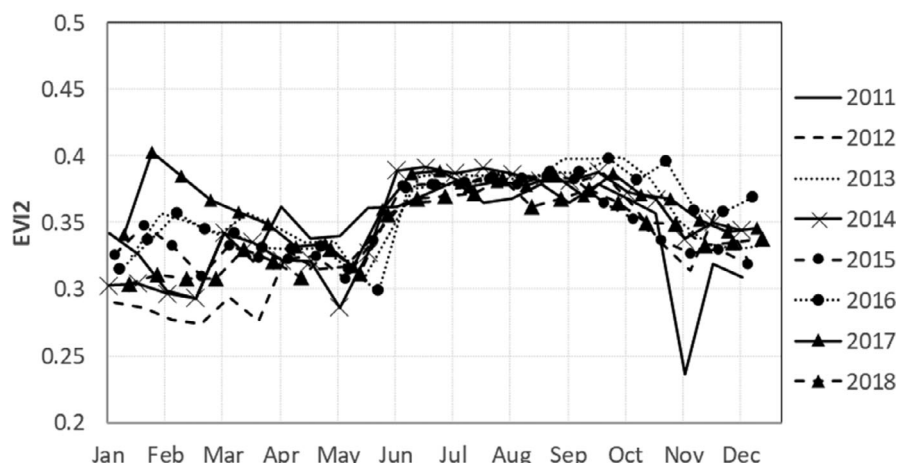
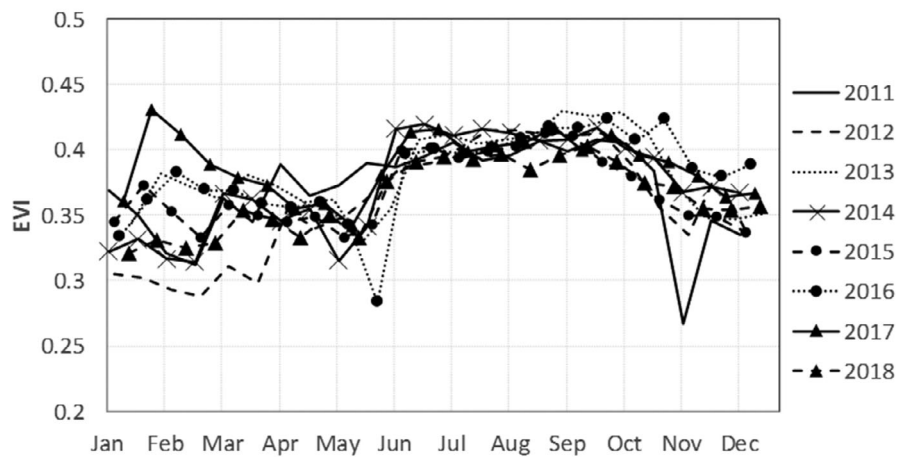


FIGURE 2 Seasonal trends of NDVI, EVI, and EVI2 from Landsat during 2011–2018. We note the high similarity between EVI and EVI2. All indices show higher VI values in the Winter/Spring (J–O)



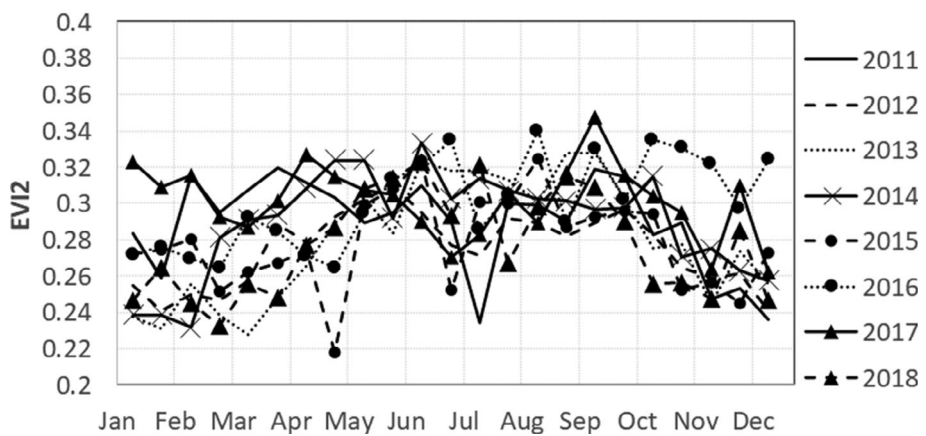
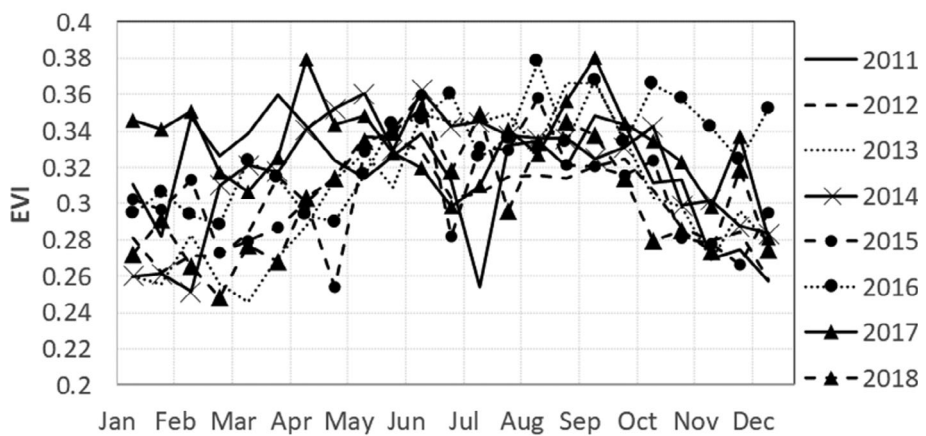
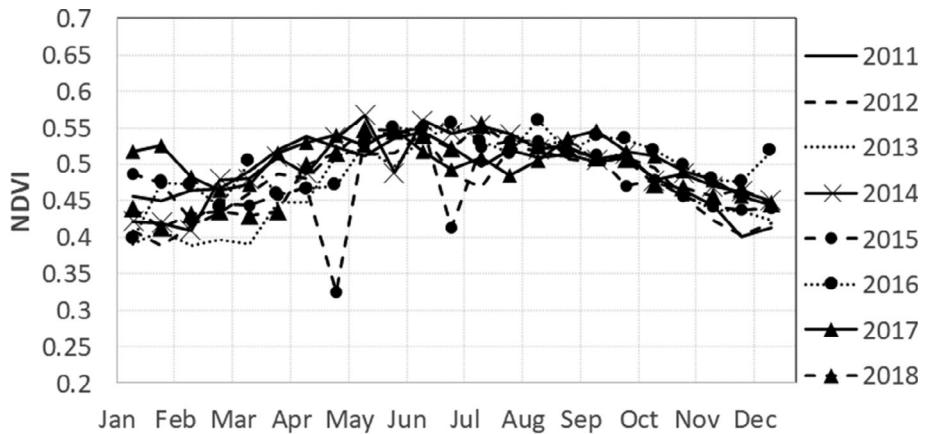
4.3 | Validation of RS-ET against SWB

RS-ET derived from Landsat (NDVI, EVI, and EVI2) and MODIS (EVI and EVI2) were compared against ground data of SWB from December 2011 to November 2012. Monthly RS-ET rates were calculated and evaluated

in comparison with SWB measurements, as presented in Figure 7. RS-ET and SWB showed similar trends throughout the study period; the highest ET occurred in summer, and lowest ET in winter, as expected.

Since the regression coefficients of daily and monthly RS-ET against SWB data was not strong ($R^2 \sim 0.41$), the black box models

FIGURE 3 Seasonal trends of NDVI, EVI, and EVI2 from MODIS during 2011–2018. All indices are highly similar as with Landsat, however, due to the mixing resulting from the larger MODIS pixel size the data is noisier, especially EVI and EVI2. All indices show higher values in the Winter/Spring months (J–O)



were tested. Based on a different number of inputs (a combination of NDVI, Landsat EVI, Landsat EVI2, MODIS EVI and MODIS EVI2), in addition to varying numbers of hidden layers (1–5), number of neurons per hidden layer (1–10), as well as different activation functions (Sigmoid or Logistic, Linear, Tanh or hyperbolic tangent), numerous scenarios (architectures) were defined and tested. Among the studied scenarios and based on the goodness of fit criteria, five topologies

were selected as the optimum MLP models. The MSE and R^2 values in both, calibration and validation, phases for selected MLPs scenarios are shown in Table 2. The high values of R^2 , as well as low values of MSE in the selected scenarios, reflect the reliable performance of MLPs models. Also, these acceptable values of the indices in the validation phase indicate the expedient process of a generalization step. Figure 8 shows the correlation as well as the equation between actual

(X-axis) and predicted (Y-axis) values in both training (left) and validation (right) steps for the selected models.

The ANN models show that SWB agrees with ET-Landsat (NDVI), ET-Landsat (EVI), ET-Landsat (EVI2), ET-MODIS (EVI) and ET-MODIS (EVI2). The high coefficient of determination, model efficiency and low RMSE confirmed a significant agreement between input/output datasets during both calibration and validation phases. According to the

goodness of fit table and performance graphs, the fifth scenario, the SWB versus ET-MODIS (EVI2), showed the best relationship with the lowest MSE ($1.4e^{-4}$ and 0.01) and highest R^2 (0.99 and 0.95) during both calibration and validation.

5 | DISCUSSION

Climate change is expected to impact urban water cycles and put extra pressure on cities that are already vulnerable to water scarcity. Many cities in arid and semi-arid lands, like Adelaide, South Australia, are exploring solutions to maintain and expand their green spaces with more sustainable strategies in the context of a changing and often drying climate. Adelaide, like all other water-stressed cities in arid and semi-arid climates, is facing mounting water scarcity pressure, particularly in recent years. This ET pressure was measured by Landsat and MODIS particularly in the summer time when demand is highest. Adelaide city managers' response to drought has been the introduction of new and stricter regulations for water usage, for example, cutting irrigation in public green spaces (Cindrić, Armour,

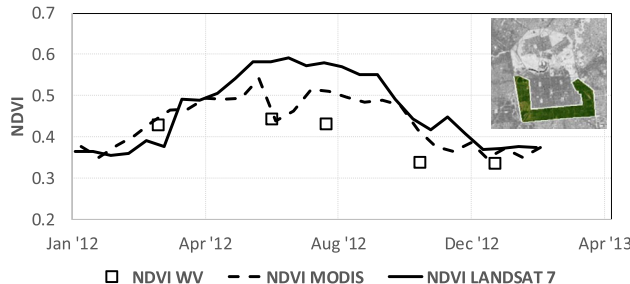


FIGURE 4 Comparison of NDVI from WV2, Landsat and MODIS in the southern half of the Adelaide Parklands

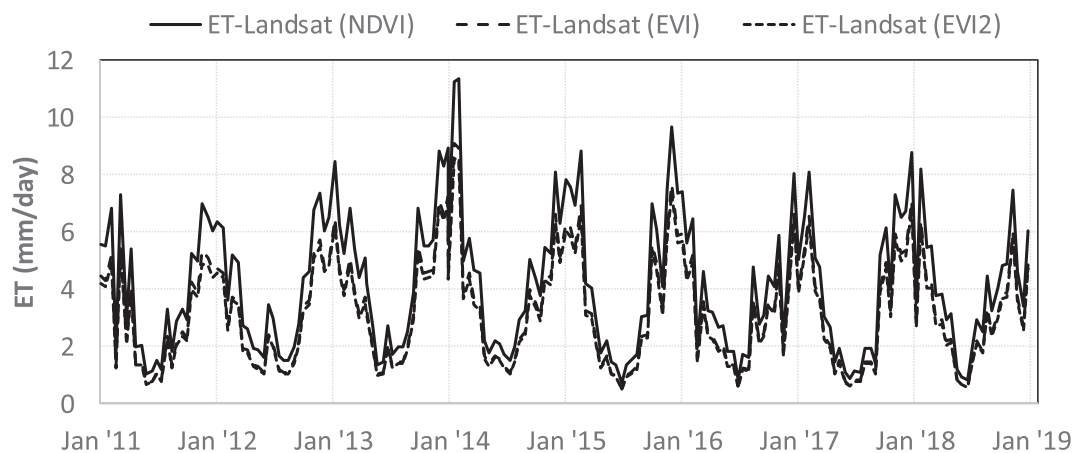


FIGURE 5 Comparison of ET-Landsat (NDVI), ET-Landsat (EVI), and ET-Landsat (EVI2) during 2011–2018 in the Adelaide Parklands

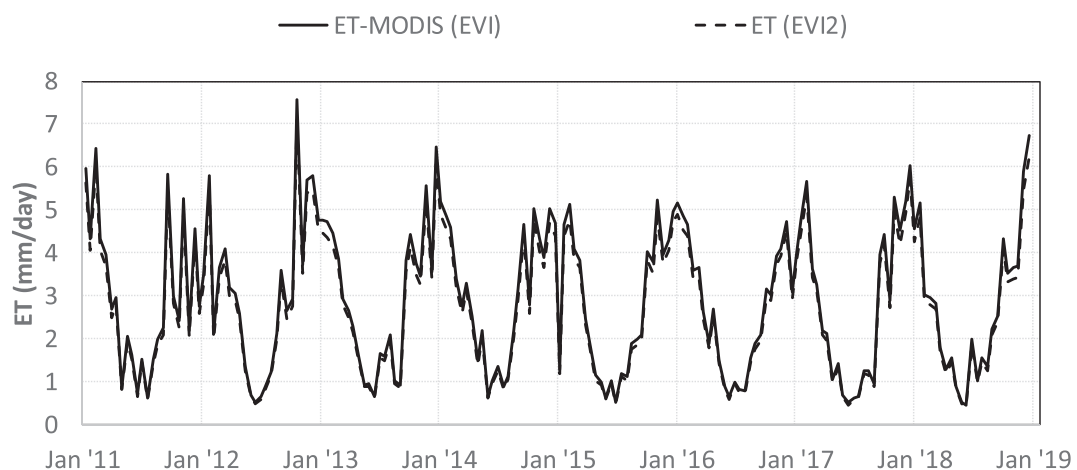


FIGURE 6 Comparison of ET-MODIS (EVI), and ET-MODIS (EVI2) during 2011–2018 in the Adelaide Parklands

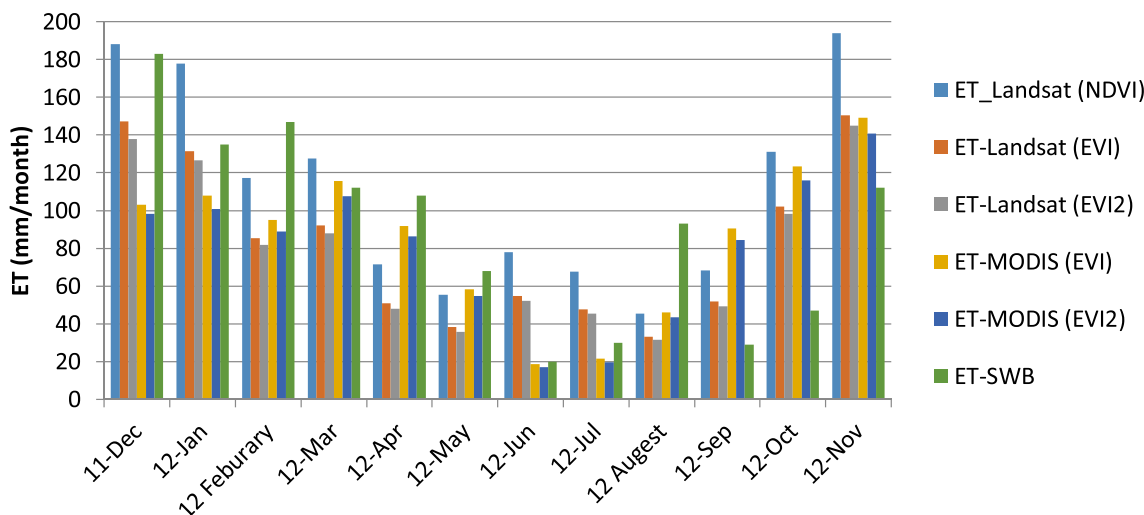


FIGURE 7 Comparison of monthly RS-ET against ground data of SWB (December 2011–November 2012)

TABLE 2 The goodness of fit indices for the optimum networks

Scenario	Input	Output	Architecture	Calibration		Validation	
				MSE	R ²	MSE	R ²
1	SWB	ET-Landsat (EVI)	1-9-1	1.1e ⁻⁴	0.99	0.05	0.97
2	SWB	ET-Landsat (EVI2)	1-7-1	0.01	0.97	0.03	0.86
3	SWB	ET-Landsat (NDVI)	1-5-1	0.02	0.97	0.02	0.98
4	SWB	ET-MODIS (EVI)	1-5-1	0.05	0.89	0.07	0.92
5	SWB	ET-MODIS (EVI2)	1-9-1	1.4e ⁻⁴	0.99	0.01	0.95

Frost, & McGregor, 2018). Trends depicted in our VIs as time-series data, throughout the years, showed how the Parklands were affected by water limitations. These trends showed minimum greenness in summer when benefits and services by green spaces are highly desired and valuable (e.g., cooling effect).

Our analysis shows a strong agreement between ET-Landsat (EVI) & ET-MODIS (EVI) ($R^2 = 0.95$) and ET-Landsat (EVI2) and ET-MODIS (EVI2) ($R^2 = 0.94$). While 30 m remains coarse for an urban setting, Landsat outperformed MODIS (250 m) by capturing the finer-scale, seasonal variation of VIs across this complex Parklands. The 250 m MODIS footprint was too coarse with poor adjacency and mixing effects. Landsat imagery makes more sense when assessing the greenness and ET of UGS with a strong recommendation for ground-based validation.

Inter- and intra-annual variation of the greenness of urban vegetation highlights the importance of an accurate assessment of ET and water demand in UGS at different times of the year. Figure 9 shows the changes in NDVI of the Parklands between two consecutive years. Some years were greener compared to their previous years, for example, 2014 compared to 2013, or 2016 compared to 2015, in the southern half of the park and some years were less greener such as 2018 compared to 2017. While these annual changes are usually profoundly impacted by the local climate and green water availability, the

restriction on blue water resources may also be playing a role in the Parklands. The Parklands is greatly dependent on blue water resources (irrigation) and must compete with other water-users in South Australia such as agriculture and industries. This suggests that maintaining the greenness of the entire Parklands year-round is probably not feasible. The city council has allowed for the drying out of a significant part of grassland areas during the summer period in the Parklands to balance and maintain enough green vegetation to maintain a certain level of service in the Parklands. Drying out grasses of the Parklands during summertime due to water shortage in Adelaide confounded the composite signal from the imagery and contributed to the observed lower Vis, considering the open-canopy nature of the park. The availability of precipitation in the wintertime while the irrigation is stopped for the entire Parklands contributed to the higher VIs observed. This may have contributed to the reshaping of the land surface phenology dynamics of the Parklands, depicting early senescence or browning (less green) in the summers and greening in the autumn–winter.

Figure 10 presents the variation of NDVIs in different years compared to the year 2011. This figure confirms that a “greening plan of Adelaide” is marginally progressing; however, values of VIs from all three satellites confirmed a gap in optimum greenness. Mean-NDVI in MODIS and Landsat were 0.49 and 0.55, respectively.

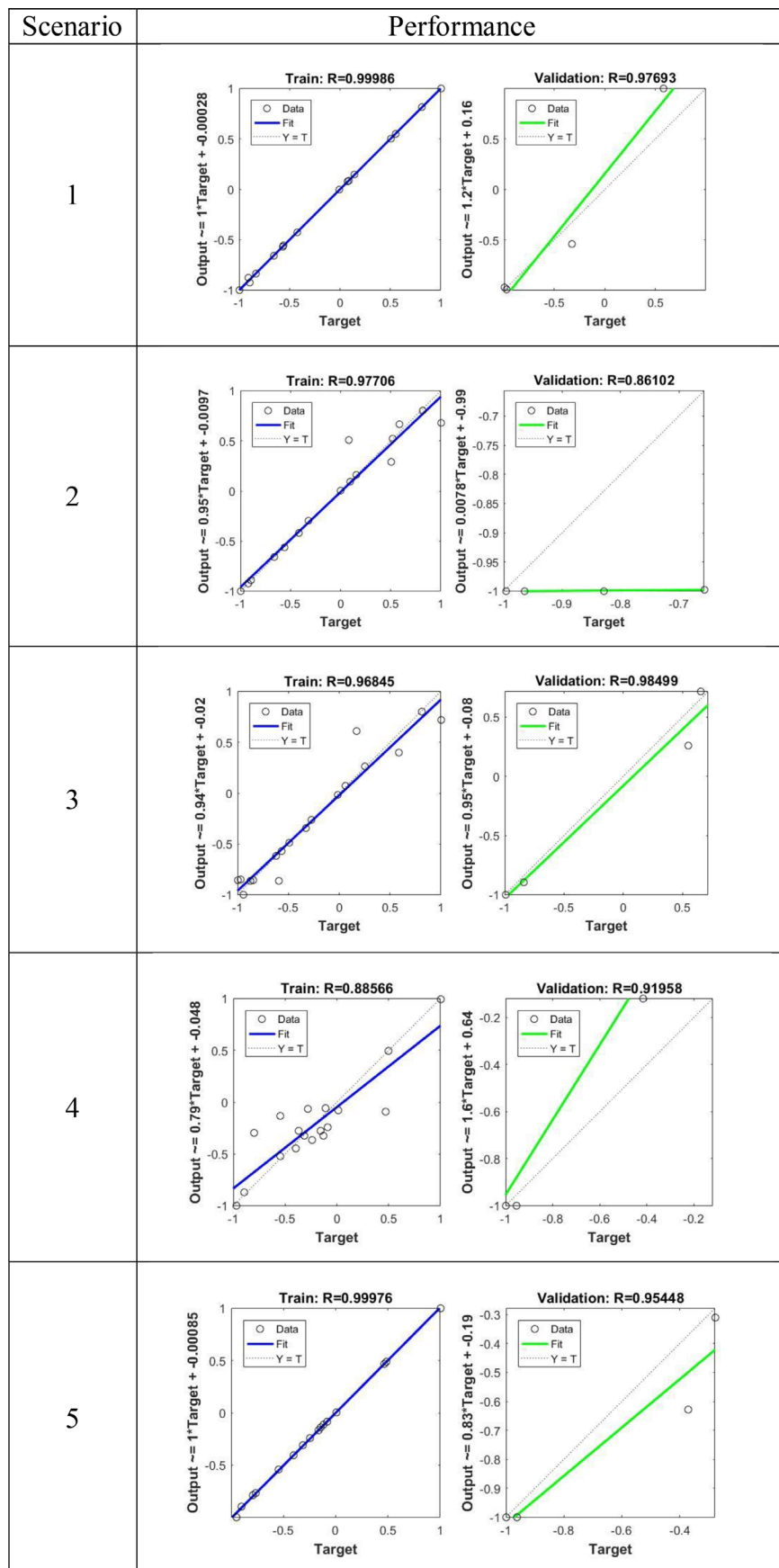


FIGURE 8 The performance of the optimum networks; the correlation between actual (x-axis) and predicted (y-axis) values in training (left) and validation (right) steps for the selected scenarios (1–5)

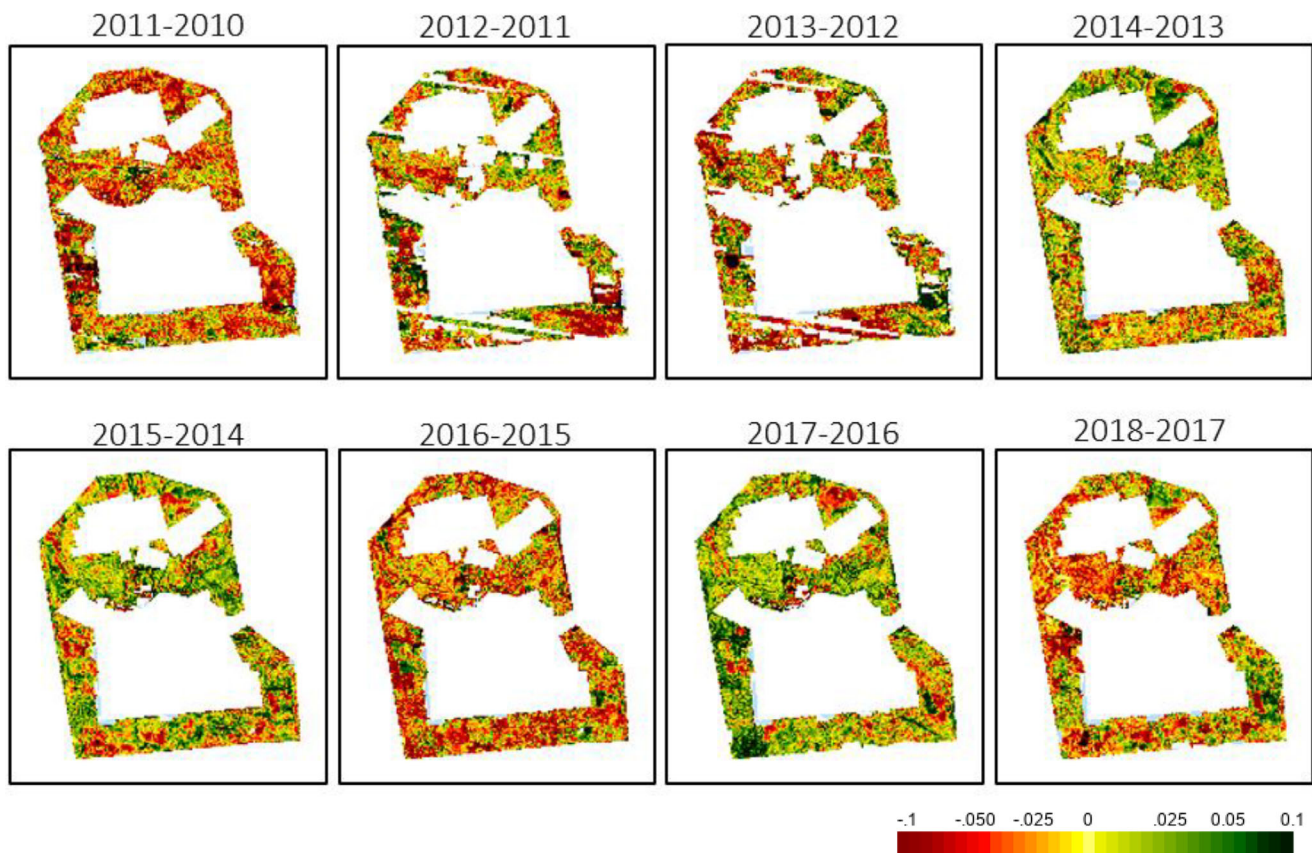


FIGURE 9 NDVI changes for two consecutive years from 2011 to 2018. The first 5 years use Landsat 7 ETM+ data and the remaining 2 years use Landsat 8 OLI

The main role of UGS is to offer a cooler and shadier retreat space, so maintaining green vegetation in parks provides a healthy habitat that is essential for both humans and animals. For instance, the cooling effect of UGS, that is both healthy and large in size, can reach up to 4°C (Aram, Higueras García, Solgi, & Mansournia, 2019). In the Parklands, the maximum urban heat island (UHI) reduction in temperature was recorded at 1.5°C in the daytime and 0.5°C in the nighttime (Guan et al., 2013; Guan et al., 2016), which is a much lower reduction in temperature than would be provided by optimum greenness of the Parklands which would benefit Adelaide. A possible solution is to have green plant cover that is comprised of drought-tolerant native species which would have lower water demand, in addition to applying the principles of water sensitive urban design (WSUD) (Chavoshi, Pezzaniti, Myers, & Sharma, 2017; Sharma et al., 2013) to free up more blue water from the limited available amount required to maintain (and possibly expand) the green cover of the Parklands.

6 | CONCLUSION

Accurate estimation of ET and water demand/water consumption for large UGS that are too large for ET monitoring from the ground

(as well as areas that are inaccessible and not cost-effective) remains critical, especially in arid and semi-arid urban environments. Measuring ET remotely will help decision-makers and water managers formulate strategies and plans for sustainable green cities across the globe. In this study, three satellites, WV2, Landsat, and MODIS were used to assess the greenness and ET of a large park, the Adelaide Parklands, a 780-ha public green space within a dry state, South Australia. Different satellite-based VIs were analysed, including those from WV2-NDVI, Landsat-NDVI, Landsat-EVI, Landsat-EVI2, MODIS-NDVI, MODIS-EVI, and MODIS-EVI2. We then compared these RS-ET with the in situ method of SWB using ANN machine learning techniques which offered a better understanding of the interactions across the parameters that define ET than regular regression analysis. Our findings point to a series of key conclusions and suggestions:

- Public and free-access satellite images can cost-effectively assist in characterizing the greenness and ET of large UGS.
- EVI2, a 2-band alternative to EVI, performed well across the three sensors, indicating its robustness and demonstrating across sensors EVI continuity
- RS-based ET performed very well and proved to be an accurate long-term monitoring tool for greenness and ET trends over large UGS. Remotely sensed estimates of ET are timely, cost-



FIGURE 10 NDVI changes over the years compared to 2011. The first 5 years use Landsat 7 ETM+ data and the remaining 2 years use Landsat 8 OLI

effective, and minimize reliance on ground-based methods. Our use of the black box models helped tease out ground-truth validation.

- While 30 m is still coarse for an urban setting, Landsat outperformed MODIS (250 m) by capturing the finer-scale and seasonal variation of VIs across the complex Parklands. The 250 m MODIS footprint was too coarse to deal with adjacency of a mixed landscape.
- The composite and divergent phenology signals resulting from trees and grasses confounded the seasonal variation in the VI profiles, implying that scale and resolution are critical in these heterogeneous urban landscapes.
- Our ET derived data captured the differences in dry, hot summers and mild, wet winters in Adelaide. This finding was captured by all of the RS-ET methods as well as the ground data estimation techniques.

Our work, based on multi-sensor remote sensing data fusion and analytical methods in an urban landscape demonstrated that these techniques are transferrable to other water-limited cities, particularly urban areas in arid and semi-arid climates, such as those in North Africa, Southern Europe, the Middle East, Southwest USA, Northern China, and Southern India. Managing water use with these novel

techniques can help identify responses to the sustainable city green space management.

ACKNOWLEDGEMENTS

This article is part of the special issue in honour of Prof. Edward P. Glenn. This paper is dedicated to Edward P. Glenn to express our sincere and deep gratitude for being such an inspiration. Edward P. Glenn was the referee of my PhD thesis, and later during my postdoc, I had the chance to work with him remotely and during my visit to the U. S. Geological Survey (USGS) and University of Arizona. It was truly a great privilege and honour to work with him and learn from him. He is sincerely missed. We thank the University of South Australia to support the in situ measurements in the Adelaide Parklands; without their help, this project would not have been possible. We are also extremely grateful to Mr. Hamed Noori, the graphic designer, for his great assistance with the graphic abstract. We wish to thank Dr. Jon Michael Hathaway for his constructive review. Any use of trade, firm, or product names is for descriptive purposes only and does not imply endorsement by the U.S. Government.

DATA AVAILABILITY STATEMENT

Data available on request due to privacy/ethical restrictions.

ORCID

- Hamideh Nouri  <https://orcid.org/0000-0002-7424-5030>
 Sina Alaghmand  <https://orcid.org/0000-0002-5568-4732>
 Alejandro Galindo  <https://orcid.org/0000-0002-3724-2586>

REFERENCES

- Aram, F., Higueras García, E., Solgi, E., & Mansournia, S. (2019). Urban green space cooling effect in cities. *Helion*, 5(4), e01339. <https://doi.org/10.1016/j.heliyon.2019.e01339>
- Barati, S., Rayegani, B., Saati, M., Sharifi, A., & Nasri, M. (2011). Comparison the accuracies of different spectral indices for estimation of vegetation cover fraction in sparse vegetated areas. *The Egyptian Journal of Remote Sensing and Space Science*, 14(1), 49–56. <https://doi.org/10.1016/j.ejrs.2011.06.001>
- Bastiaanssen, W. G. M., Menenti, M., Feddes, R. A., & Holtslag, A. A. M. (1998). A remote sensing surface energy balance algorithm for land (SEBAL). 1. Formulation. *Journal of Hydrology*, 212–213, 198–212. [https://doi.org/10.1016/S0022-1694\(98\)00253-4](https://doi.org/10.1016/S0022-1694(98)00253-4)
- Chavoshi, S., Pezzaniti, D., Myers, B., & Sharma, A. K. (2017, March). Modelling storm water management for Water Sensitive Urban Design Using SUSTAIN. Paper presented at the 13th International Drainage Workshop of ICID, Ahwaz, Iran.
- Cindrić, H., Armour, T., Frost, J., & McGregor, A. (2018). *Cities alive; rethinking cities in arid environments*. Dubai, UAE: Dubai Media City.
- Costanza, R., & Liu, S. (2014). Ecosystem services and environmental governance: Comparing China and the U.S. *Asia & the Pacific Policy Studies*, 1(1), 160–170. <https://doi.org/10.1002/app5.16>
- Elgström, L., Erman, M., Klindworth, K., & Koenig, C. (2014). *European cities moving towards climate neutrality practices, tools and policies*. Stockholm, Sweden.
- Evans, R. G., & Sadler, E. J. (2008). Methods and technologies to improve efficiency of water use. *Water Resources Research*, 44(7), W00E04. <https://doi.org/10.1029/2007wr006200>
- García, M., Sandholt, I., Ceccato, P., Ridder, M., Mougin, E., Kerfoot, L., ... Domingo, F. (2013). Actual evapotranspiration in drylands derived from in-situ and satellite data: Assessing biophysical constraints. *Remote Sensing of Environment*, 131, 103–118. <https://doi.org/10.1016/j.rse.2012.12.016>
- Glenn, E. P., Mexicano, L., Garcia-Hernandez, J., Nagler, P. L., Gomez-Sapiens, M. M., Tang, D., ... Zamora-Arroyo, F. (2013). Evapotranspiration and water balance of an anthropogenic coastal desert wetland: Responses to fire, inflows and salinities. *Ecological Engineering*, 59, 176–184. <https://doi.org/10.1016/j.ecoleng.2012.06.043>
- Glenn, E. P., Nagler, P. L., & Huete, A. R. (2010). Vegetation index methods for estimating evapotranspiration by remote sensing. *Surveys in Geophysics*, 31(6), 531–555. <https://doi.org/10.1007/s10712-010-9102-2>
- Glenn, E. P., Neale, C. M. U., Hunsaker, D. J., & Nagler, P. L. (2011). Vegetation index-based crop coefficients to estimate evapotranspiration by remote sensing in agricultural and natural ecosystems. *Hydrological Processes*, 25(26), 4050–4062. <https://doi.org/10.1002/hyp.8392>
- Glenn, E. P., Scott, R. L., Nguyen, U., & Nagler, P. L. (2015). Wide-area ratios of evapotranspiration to precipitation in monsoon-dependent semiarid vegetation communities. *Journal of Arid Environments*, 117, 84–95. <https://doi.org/10.1016/j.jaridenv.2015.02.010>
- Gómez, C., White, J. C., & Wulder, M. A. (2016). Optical remotely sensed time series data for land cover classification: A review. *ISPRS Journal of Photogrammetry and Remote Sensing*, 116, 55–72. <https://doi.org/10.1016/j.isprsjprs.2016.03.008>
- Grekousis, G., Mountakis, G., & Kavouras, M. (2015). An overview of 21 global and 43 regional land-cover mapping products. *International Journal of Remote Sensing*, 36(21), 5309–5335. <https://doi.org/10.1080/01431161.2015.1093195>
- Groeneveld, D. P., Baugh, W. M., Sanderson, J. S., & Cooper, D. J. (2007). Annual groundwater evapotranspiration mapped from single satellite scenes. *Journal of Hydrology*, 344(1), 146–156. <https://doi.org/10.1016/j.jhydrol.2007.07.002>
- Guan, H., Bennett, J., Ewenz, C., Benger, S., Vinodkumar, Z. S., Clay, R., & Soebarto, V. (2013). *Characterisation, interpretation and implications of the Adelaide Urban Heat Island*. Adelaide, Australia: Flinders University.
- Guan, H., Kumar, V., Clay, R., Kent, C., Bennett, J., Ewenz, C., ... Simmons, C. T. (2016). Temporal and spatial patterns of air temperature in a coastal city with a slope base setting. *Journal of Geophysical Research: Atmospheres*, 121(10), 5336–5355. <https://doi.org/10.1002/2016jd025139>
- Gutman, G., & Ignatov, A. (1998). The derivation of the green vegetation fraction from NOAA/AVHRR data for use in numerical weather prediction models. *International Journal of Remote Sensing*, 19(8), 1533–1543. <https://doi.org/10.1080/014311698215333>
- Hilaire, R., Arnold, M., Wilkerson, D., Devitt, D., Hurd, B., Lesikar, B., ... Zoldoske, D. (2008). Efficient water use in residential urban landscapes. *HortScience*, 43(7), 2081–2092.
- Huete, A., Didan, K., Miura, T., Rodriguez, E. P., Gao, X., & Ferreira, L. G. (2002). Overview of the radiometric and biophysical performance of the MODIS vegetation indices. *Remote Sensing of Environment*, 83(1), 195–213. [https://doi.org/10.1016/S0034-4257\(02\)00096-2](https://doi.org/10.1016/S0034-4257(02)00096-2)
- Huete, A., Didan, K., van Leeuwen, W., Miura, T., & Glenn, E. (2011). MODIS vegetation indices. In B. Ramachandran, C. O. Justice, & M. J. Abrams (Eds.), *Land remote sensing and global environmental change: NASA's earth observing system and the science of ASTER and MODIS* (pp. 579–602). New York, NY: Springer New York.
- Irmak, S., & Haman, D. Z. (2003). *Evapotranspiration: Potential or Reference?* Gainesville, FL: The Institute of Food and Agricultural Sciences (IFAS).
- Jarchow, C. J., Didan, K., Barreto-Muñoz, A., Nagler, P. L., & Glenn, E. P. (2018). Application and comparison of the MODIS-derived enhanced vegetation index to VIIRS, Landsat 5 TM and Landsat 8 OLI platforms: A case study in the arid Colorado River Delta, Mexico. *Sensors*, 18(5), 1546.
- Jarchow, C. J., Waugh, W. J., Didan, K., Barreto-Muñoz, A., Herrmann, S., & Nagler, P. L. (2020). Vegetation-groundwater dynamics at a former uranium mill site following invasion of a biocontrol agent: A time series analysis of landsat normalized difference vegetation index (NDVI) data. *Hydrological Processes*, 34(8), <http://dx.doi.org/10.1002/hyp.13772>.
- Jiang, Z., Huete, A. R., Didan, K., & Miura, T. (2008). Development of a two-band enhanced vegetation index without a blue band. *Remote Sensing of Environment*, 112(10), 3833–3845. <https://doi.org/10.1016/j.rse.2008.06.006>
- Jiapaer, G., Chen, X., & Bao, A. (2011). A comparison of methods for estimating fractional vegetation cover in arid regions. *Agricultural and Forest Meteorology*, 151(12), 1698–1710. <https://doi.org/10.1016/j.agrmet.2011.07.004>
- Kim, Y., Huete, A. R., Miura, T., & Jiang, Z. (2010). Spectral compatibility of vegetation indices across sensors: Band decomposition analysis with Hyperion data. *Journal of Applied Remote Sensing*, 4, 043520.
- Li, F., Sutton, P., & Nouri, H. (2018). Planning green space for climate change adaptation and mitigation: A review of green space in the Central City of Beijing. *Urban and Regional Planning*, 3(2), 55–63. <https://doi.org/10.11648/j.upr.20180302.13>
- Li, F., Sutton, P. C., Anderson, S. J., & Nouri, H. (2017). Planning green space in Adelaide city: Enlightenment from green space system planning of Fuzhou city (2015–2020). *Australian Planner*, 54(2), 126–133. <https://doi.org/10.1080/07293682.2017.1345962>
- Litvak, E., Bijoor, N. S., & Pataki, D. E. (2014). Adding trees to irrigated turfgrass lawns may be a water-saving measure in semi-arid environments. *Ecohydrology*, 7(5), 1314–1330. <https://doi.org/10.1002/eco.1458>

- Litvak, E., Manago, K. F., Hogue, T. S., & Pataki, D. E. (2017). Evapotranspiration of urban landscapes in Los Angeles, California at the municipal scale. *Water Resources Research*, 53(5), 4236–4252. <https://doi.org/10.1002/2016wr020254>
- Litvak, E., & Pataki, D. E. (2016). Evapotranspiration of urban lawns in a semi-arid environment: An in situ evaluation of microclimatic conditions and watering recommendations. *Journal of Arid Environments*, 134, 87–96. <https://doi.org/10.1016/j.jaridenv.2016.06.016>
- Maheng, D., Ducton, I., Lauwaet, D., Zevenbergen, C., & Pathirana, A. (2019). The sensitivity of urban heat island to urban green space—A model-based study of City of Colombo, Sri Lanka. *Atmosphere*, 10(3), 151.
- Mini, C., Hogue, T. S., & Pincetl, S. (2014). Estimation of residential outdoor water use in Los Angeles, California. *Landscape and Urban Planning*, 127, 124–135. <https://doi.org/10.1016/j.landurbplan.2014.04.007>
- Montandon, L. M., & Small, E. E. (2008). The impact of soil reflectance on the quantification of the green vegetation fraction from NDVI. *Remote Sensing of Environment*, 112(4), 1835–1845. <https://doi.org/10.1016/j.rse.2007.09.007>
- Nagler, P. L., Cleverly, J., Glenn, E., Lampkin, D., Huete, A., & Wan, Z. (2005). Predicting riparian evapotranspiration from MODIS vegetation indices and meteorological data. *Remote Sensing of Environment*, 94(1), 17–30. <https://doi.org/10.1016/j.rse.2004.08.009>
- Nagler, P. L., Doody, T. M., Glenn, E. P., Jarchow, C. J., Barreto-Muñoz, A., & Didan, K. (2016). Wide-area estimates of evapotranspiration by red gum (*Eucalyptus camaldulensis*) and associated vegetation in the Murray-Darling River Basin, Australia. *Hydrological Processes*, 30(9), 1376–1387. <https://doi.org/10.1002/hyp.10734>
- Nagler, P. L., Glenn, E. P., Nguyen, U., Scott, R. L., & Doody, T. (2013). Estimating riparian and agricultural actual evapotranspiration by reference evapotranspiration and MODIS enhanced vegetation index. *Remote Sensing*, 5, 3849–3871.
- Nagler, P. L., Jarchow, C. J., & Glenn, E. P. (2018). Remote sensing vegetation index methods to evaluate changes in greenness and evapotranspiration in riparian vegetation in response to the Minute 319 environmental pulse flow to Mexico. *Proc. IAHS*, 380, 45–54. <https://doi.org/10.5194/piahs-380-45-2018>
- Nagler, P. L., Nguyen, U., Bateman, H. L., Jarchow, C. J., Glenn, E. P., Waugh, W. J., ... van Riper III C. (2018). Northern tamarisk beetle (*Diorhabda carinulata*) and tamarisk (*Tamarix spp.*) interactions in the Colorado River basin. *Restoration Ecology*, 26(2), 348–359. <https://doi.org/10.1111/rec.12575>
- Nguyen, U., Glenn, E. P., Nagler, P. L., & Scott, R. L. (2015). Long-term decrease in satellite vegetation indices in response to environmental variables in an iconic desert riparian ecosystem: The Upper San Pedro, Arizona, United States. *Ecohydrology*, 8(4), 610–625. <https://doi.org/10.1002/eco.1529>
- Nouri, H., Anderson, S., Sutton, P., Beecham, S., Nagler, P., Jarchow, C. J., & Roberts, D. A. (2017). NDVI, scale invariance and the modifiable areal unit problem: An assessment of vegetation in the Adelaide Parklands. *Science of the Total Environment*, 584–585, 11–18. <https://doi.org/10.1016/j.scitotenv.2017.01.130>
- Nouri, H., Beecham, S., Anderson, S., Hassanli, A. M., & Kazemi, F. (2015). Remote sensing techniques for predicting evapotranspiration from mixed vegetated surfaces. *Urban Water Journal*, 12(5), 380–393. <https://doi.org/10.1080/1573062X.2014.900092>
- Nouri, H., Beecham, S., Anderson, S., & Nagler, P. (2014). High spatial resolution WorldView-2 imagery for mapping NDVI and its relationship to temporal urban landscape evapotranspiration factors. *Remote Sensing*, 6(1), 580–602.
- Nouri, H., Beecham, S., Hassanli, A. M., & Ingleton, G. (2013). Variability of drainage and solute leaching in heterogeneous urban vegetation environments. *Hydrology and Earth System Sciences*, 17, 4339–4347.
- Nouri, H., Beecham, S., Hassanli, A. M., & Kazemi, F. (2013). Water requirements of urban landscape plants: A comparison of three factor-based approaches. *Ecological Engineering*, 57, 276–284. <https://doi.org/10.1016/j.ecoleng.2013.04.025>
- Nouri, H., Beecham, S., Kazemi, F., & Hassanli, A. M. (2013). A review of ET measurement techniques for estimating the water requirements of urban landscape vegetation. *Urban Water Journal*, 10(4), 247–259. <https://doi.org/10.1080/1573062X.2012.726360>
- Nouri, H., Chavoshi Borujeni, S., & Hoekstra, A. Y. (2019). The blue water footprint of UGS: An example for Adelaide, Australia. *Landscape and Urban Planning*, 190, 103613. <https://doi.org/10.1016/j.landurbplan.2019.103613>
- Nouri, H., Glenn, E. P., Beecham, S., Chavoshi Borujeni, S., Sutton, P., Alaghmand, S., ... Nagler, P. (2016). Comparing three approaches of evapotranspiration estimation in mixed urban vegetation: Field-based, remote sensing-based and observational-based methods. *Remote Sensing*, 8(6), 492.
- Ouyang, Y., Wentz, E. A., Ruddell, B. L., & Harlan, S. L. (2014). A multi-scale analysis of single-family residential water use in the Phoenix metropolitan area. *JAWRA Journal of the American Water Resources Association*, 50(2), 448–467. <https://doi.org/10.1111/jawr.12133>
- Qiu, G. Y., Zou, Z., Li, X., Li, H., Guo, Q., Yan, C., & Tan, S. (2017). Experimental studies on the effects of green space and evapotranspiration on urban heat island in a subtropical megacity in China. *Habitat International*, 68, 30–42. <https://doi.org/10.1016/j.habitatint.2017.07.009>
- Revelli, R., & Porporato, A. (2018). Ecohydrological model for the quantification of ecosystem services provided by urban street trees. *Urban Ecosystem*, 21(3), 489–504. <https://doi.org/10.1007/s11252-018-0741-2>
- Sharma, A. K., Pezzaniti, D., Myres, B., Chacko, P., Tjandraatmadja, G., Cook, S., ... Walton, A. (2013, November). *The role of water sensitive urban design in supplementing urban water services*. Paper presented at the International Water Week Conference, Amsterdam, the Netherlands.
- Shojaei, P., Gheysari, M., Nouri, H., Myers, B., & Esmaeili, H. (2018). Water requirements of urban landscape plants in an arid environment: The example of a botanic garden and a forest park. *Ecological Engineering*, 123, 43–53. <https://doi.org/10.1016/j.ecoleng.2018.08.021>
- Skelhorn, C. P., Lindley, S., & Levermore, G. (2018). Urban greening and the UHI: Seasonal trade-offs in heating and cooling energy consumption in Manchester, UK. *Urban Climate*, 23, 173–187. <https://doi.org/10.1016/j.uclim.2017.02.010>
- Storey, J., Scaramuzza, P. L., & Schmidt, G. E. (2005, October). *Landsat 7 scan line corrector-off gap-filled product development*. Paper presented at the Pecora 16 “Global Priorities in Land Remote Sensing,” Sioux Falls, SD.
- Su, Z. (2002). The surface energy balance system (SEBS) for estimation of turbulent heat fluxes. *Hydrology and Earth System Sciences*, 6(1), 85–100. <https://doi.org/10.5194/hess-6-85-2002>
- Velpuri, N. M., & Senay, G. B. (2017). Partitioning evapotranspiration into green and blue water sources in the conterminous United States. *Scientific Reports*, 7(1), 6191. <https://doi.org/10.1038/s41598-017-06359-w>
- Wagner, I., & Zalewski, M. (2009). Ecohydrology as a basis for the sustainable city strategic planning: Focus on Lodz, Poland. *Reviews in Environmental Science and Bio/Technology*, 8(3), 209–217. <https://doi.org/10.1007/s11157-009-9169-8>
- Xian, G., Shi, H., Dewitz, J., & Wu, Z. (2019). Performances of WorldView 3, Sentinel 2, and Landsat 8 data in mapping impervious surface. *Remote Sensing Applications: Society and Environment*, 15, 100246. <https://doi.org/10.1016/j.rsase.2019.100246>
- Yebra, M., Van Dijk, A., Leuning, R., Huete, A., & Guerschman, J. P. (2013). Evaluation of optical remote sensing to estimate actual evapotranspiration and canopy conductance. *Remote Sensing of Environment*, 129, 250–261. <https://doi.org/10.1016/j.rse.2012.11.004>
- Zeng, X., Dickinson, R. E., Walker, A., Shaikh, M., DeFries, R. S., & Qi, J. (2000). Derivation and evaluation of global 1-km fractional

- vegetation cover data for land modeling. *Journal of Applied Meteorology*, 39(6), 826–839. [https://doi.org/10.1175/1520-0450\(2000\)039<0826:daeogk>2.0.co;2](https://doi.org/10.1175/1520-0450(2000)039<0826:daeogk>2.0.co;2)
- Zhang, X., Liao, C., Li, J., & Sun, Q. (2013). Fractional vegetation cover estimation in arid and semi-arid environments using HJ-1 satellite hyperspectral data. *International Journal of Applied Earth Observation and Geoinformation*, 21, 506–512. <https://doi.org/10.1016/j.jag.2012.07.003>

How to cite this article: Nouri H, Nagler P, Chavoshi Borujeni S, et al. Effect of spatial resolution of satellite images on estimating the greenness and evapotranspiration of urban green spaces. *Hydrological Processes*. 2020;34:3183–3199. <https://doi.org/10.1002/hyp.13790>